Doppler-Shifted Cyclotron Absorption of Electron Bernstein Waves via $N_\parallel$-Upshift in a Tokamak Plasma

T. Maekawa,[1] T. Kobayashi,[1] S. Yamaguchi,[2] K. Yoshinaga,[2] H. Igami,[1] M. Uchida,[1] H. Tanaka,[1]
M. Asakawa,[2] and Y. Terumichi[2]

[1]*Graduate School of Energy Science, Kyoto University, Kyoto 606-8502, Japan*
[2]*Department of Physics, Kyoto University, Kyoto 606-8502, Japan*

Extraordinary (X) waves are perpendicularly injected for electron Bernstein (B) wave heating into an Ohmically heated plasma from the inboard side in the WT-3 tokamak. Measurements show that absorption does not take place at the electron cyclotron resonance layer nor the upper hybrid resonance layer, but does happen midway between them. This is consistent with the ray tracing prediction, i.e., the poloidal field and poloidal inhomogeneity of toroidal field lead the B waves to have a large parallel refractive index $N_\parallel$ (>1), and the B waves are damped away via the Doppler-shifted cyclotron resonance.

Recently, there arises considerable interest in excitation and propagation processes of B waves in relationship to electron cyclotron heating (ECH), current drive (ECCD), and diagnostics of overdense plasmas in stellarators [1,2] and spherical tokamaks [3–5], since they have no density limit for propagation and have the potential ability to heat and diagnose high density plasmas, where usual electromagnetic waves cannot propagate. They are electrostatic waves in magnetized plasmas, and have large refractive indices $N \gg 1$ in almost perpendicular direction to the magnetic field. The largeness of N makes B waves sensitive to the direction of the magnetic field. When the index vector deviates from the perpendicular direction, Doppler-shifted cyclotron resonance takes place for the thermal electrons and the B waves are cyclotron damped away. Although these characters were partly verified in a low temperature plasma in a homogeneous magnetic field [6], there are few experiments in high temperature toroidal plasmas, where the magnetic fields are inhomogeneous and complicated. In toroidal plasmas with the toroidal and poloidal magnetic fields, B_t and B_p, the parallel index is given by $N_\parallel = (N_p B_p + N_t B_t)/B \simeq (N_p B_p)/B_t + N_t$, where N_p and N_t are the poloidal and toroidal indices, respectively. Ray tracing studies of the B waves based on the geometrical optics predict that the poloidal contribution, $(N_p B_p)/B_t$, can become large during propagation in contrast to the cases of electromagnetic modes [4,5,7]. With a large $N_\parallel$, B waves are damped away apart from the electron cyclotron resonance (ECR) layer via Doppler-shifted cyclotron resonance, which may have a significant effect on the power deposition profile. Furthermore, high $N_\parallel$ waves are advantageous for efficient ECCD [5,8].

In this Letter, we present the first experimental results which show that the $N_\parallel$ upshift of B waves does occur consistently with the ray tracing prediction. We employ perpendicular injection of X waves to the toroidal field from the inboard side for B wave excitation. In this case, $N_\parallel$ stems from $(N_p B_p)/B_t$ alone in contrast to the oblique injection in the W7-AS experiment [1].

The experiments were carried out in the WT-3 tokamak, with major and minor radii of $R_0 = 65$ and $a = 20$ cm, respectively. The toroidal field is $B_{t0} < 1.75$ T at $R = R_0$. The ECH power is generated by a gyrotron (48 GHz, 150 kW maximum), transmitted to a top port via corrugated wave guides, guided into the vacuum vessel through a ceramic vacuum window, and injected perpendicularly to the toroidal field in the form of a Gaussian beam by a couple of mirrors toward a corrugated polarizer attached on the inboard vessel wall (Fig. 1). The beam radius defined at the e^{-1} power density is 2 cm on the polarizer. The wave electric field is parallel to the toroidal field (O mode), and the wave is mode converted into X mode by the polarizer and reflected back toward the plasma. The design value of mode conversion efficiency is more than 96% for the present experiment. The launching mirror focuses and steers the O waves in order to compensate the refraction in the plasma.
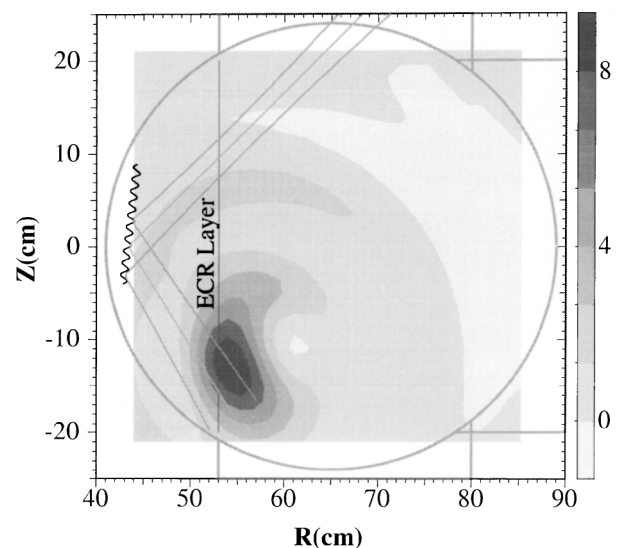

FIG. 1.   Soft x-ray CT image of ECR plasma. Solid lines show the axis and envelope of the injected Gaussian beam.

We first produced ECR plasmas with the toroidal field alone for the test of the ECH system with a low power of $P_{EC} \sim 10$ kW. The ECR plasmas were observed with five soft x-ray (SX) detector arrays, which surround the plasma poloidally. A typical spatial structure of the SX emissivity during injection is reconstructed by computerized tomography (CT) and shown in Fig. 1, which shows that an ECR plasma appears near the crossing point of the reflected X wave ray on the ECR layer. Since the line averaged electron density is as low as $\overline{n_e} \sim 1.0 \times 10^{12}$ cm^{-3} for the present case of low P_{EC}, no refractive effect may appear for the O and X waves except for the peak position of SX emissivity. No plasma is observed near the crossing point of the injected O wave on the ECR layer. Thus, it appears that the ECH system for injection of X waves from the high field side works well.

ECH power at $P_{EC} \simeq 100$ kW was injected into an Ohmically heated plasma with the plasma current $I_p \simeq 60$ kA and the density $\overline{n_e} \simeq 1.1 \times 10^{13}$ cm^{-3} as shown in Fig. 2. With P_{EC} injection, the loop voltage decreases from $V_L \simeq 1.9$ to 1.5 V in accord with the increase of SX signal from a detector looking at the whole plasma cross section, suggesting that bulk electron heating occurs. With P_{EC} injection, the density decreases in accord with the increase of $H\alpha$ signal, indicating that particle confinement deteriorates. A hard x-ray (HX) signal appears $\sim 2-3$ ms after P_{EC} is turned on, indicating production of suprathermal electrons. The electron cyclotron emission (ECE) also

increases but does not attain a steady level during the ECH pulse. The decay time of the ECE signal after ECH is turned off is composed of fast and slow time constants. The fast one is nearly the same as those of the V_L and SX signals, suggesting that it comes from the decay of the bulk electron temperature. The slow one may be due to the decay of suprathermal electrons. Although the HX and ECE signals indicate production of fast electrons, both the loop voltage and the SX intensity keep constant values during ECH pulse, suggesting that the bulk electron temperature keeps a constant profile and that the amount of fast electrons is not significant.

The incremental SX emissivity profiles at the onset of ECH are found to make an annular ring on the plasma cross section as shown in Fig. 3(a). The local SX emissivity depends on both plasma density and electron temperature. The time constants of V_L change at ECH turned on and off, which may be a good measure of the time constant of bulk electron temperature change, is ~ 1 ms and much shorter than those of density change as shown in Fig. 2. We, therefore, take a short time difference of 0.5 ms in
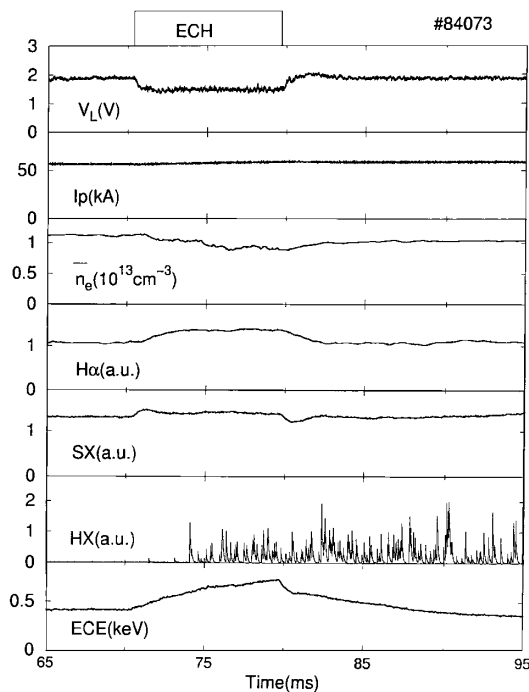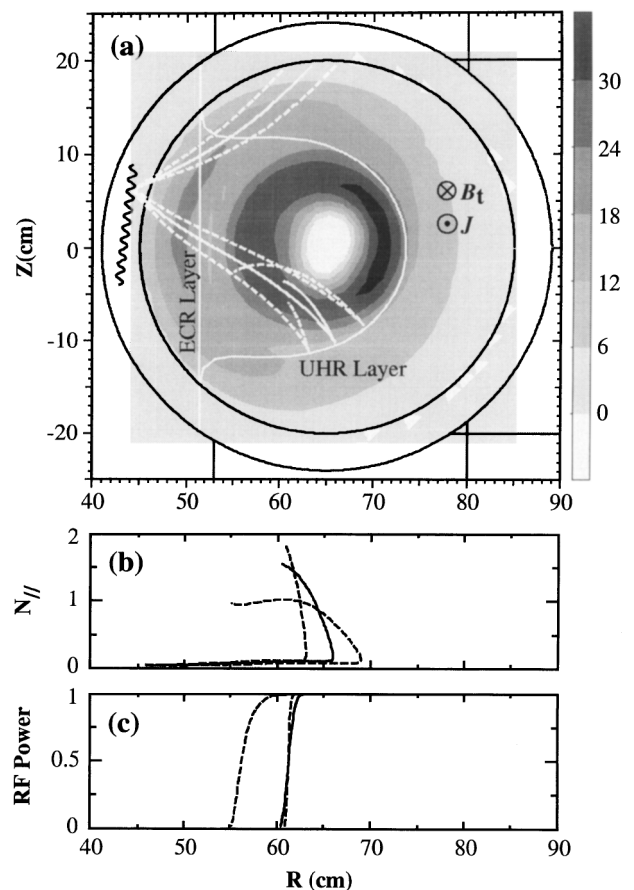

FIG. 2. Temporal evolution of plasma parameters during a B wave heating discharge. From top: loop voltage, plasma current, central chord line averaged density, intensity of $H\alpha$, soft x-ray, hard x-ray, and second harmonic ECE signal from the plasma center.

FIG. 3. Incremental SX image at the onset of B wave heating, and the ray trajectories. Variation of (b) $N_\parallel$ and (c) wave power along the trajectories. Dotted lines are for peripheral rays and the solid line is for the central ray. Calculation parameters are $n_0 = 2.16 \times 10^{13}$ cm^{-3}, $T_0 = 480$ eV, $I_p = 60$ kA, $\nu_n = 2$, $\nu_T = 3$, and $\nu_J = 4.5$.

producing the incremental SX profiles in order to suppress the effect of the density change on the SX profile. Thus, the annular reflects an essential change of the electron temperature profile. The decremental SX emissivity profiles at the ECH turned off are also found to have nearly the same annular ring. An $m = 1$ structure always appears with a hill at the low field side as shown in Fig. 3(a), which may be ascribed to the slight shift of the plasma column to the low field side (~ 0.7 mm) by ECH.

The ray trajectories in a toroidal geometry are calculated by the ray tracing code described in Ref. [7]. The radial profiles of electron density, temperature, and plasma current assume the form $n_e/n_0 = T_e/T_0 = J/J_0 = [1 - (r/a)^2]^\nu$, where the central values denoted by the subscript 0 and the indices ν are fitted to the experimental values, respectively. The poloidal field is approximated by $B_p = (\mu_0/r) \int_0^r Jx\,dx$. In Fig. 3(a), three trajectories projected on the poloidal cross section are plotted to simulate the injected Gaussian beam. The injected O waves make curved trajectories due to the refraction effect, arrive at the upper part of the polarizer, and are mode converted to X waves. The X waves, then, propagate to the upper hybrid resonance (UHR) layer and are mode converted into B waves, which propagate backward and are damped away before arriving at the ECR layer by Doppler-shifted cyclotron absorption due to the upshift of $N_\parallel$, as shown in Figs. 3(b) and 3(c). It is found that the parallel velocity of resonance electrons at the absorption point is $v_\parallel \equiv c(1 - \Omega_e/\omega)/N_\parallel \simeq 2.6v_t$, where $v_t = \sqrt{2T_e/m}$ is the local electron thermal velocity. Here, the spatial damping rate of the B waves becomes quite high since the group velocity, which is proportional to the electron thermal velocity, is low. Wave power is, therefore, quickly and completely absorbed once the damping takes place. Cyclotron damping of the O and X waves is both negligibly small, since both the electron density and the temperature are low at the ECR layer. In these low current discharges, the poroidal field is as low as $B_p \sim B_t/20$; therefore, the coupling fraction to the other mode at the injection points is negligible ($\sim 0.3\%$) for the linearly polarized wave parallel (O) or perpendicular (X) to the toroidal field.

In Fig. 3(a), the annular ring does not cross the ECR layer, which excludes the possibility that the B waves reach the ECR layer without $N_\parallel$ upshift and are cyclotron damped there. At the UHR resonance layer, the group velocity of B waves is quite small and the collisional damping may become effective if the electron temperature is low. However, numerical calculations show that they are negligibly small for the present case of electron temperature of $T_e > 100$ eV. Actually, the mode conversion area of the rays is beside the SX annular ring and the calculated power deposition regions are just on the annular ring of the incremental SX image, as shown in Fig. 3(a).

A power deposition profile was also investigated by the second harmonic ECE by using a filter bank ra-

diometer composed of two frequency bands (67–83 and 83–99 GHz). Each band has 16 channels with a 1 GHz bandwidth for each channel. Unfortunately, the upper band becomes dead during the ECH pulse, which may be due to a parasitic output at the second harmonic frequency of $f = 96$ GHz. Therefore, radial radiation temperature profiles just after ECH is turned off for various ECH pulse lengths, as well as just before the ECH pulse, are plotted in Fig. 4(c), where a peak denoted by an arrow appears with ECH at $R = 55-60$ cm, coincident with the location of the SX annular ring in Fig. 3(a). In Figs. 4(a) and 4(b) are plotted time evolutions of ECE signals from inboard and outboard sides for various ECH pulse lengths, respectively. Although nonthermal emission dominates in the case of long ECH pulses, no nonthermal effect appears in the strong field side ECE signals for a short pulse of 1 ms, as shown in Fig. 4(a). Namely, the decay curve can be fitted by a single e-folding time constant of $\tau_d = 0.9$ ms.

A decremental ECE temperature profile at the inboard side between a short time interval of 0.1 ms just after the 1 ms ECH pulse is plotted in Fig. 5(b). The power deposition profiles of B waves from multiray tracing calculations for various current profiles are plotted in Fig. 5(a), showing coincidence with the decremental ECE profile for a wide range of indices of $\nu_J = \sim 3-6$. The change of electron energy contents during this short time interval is estimated to be 5.7 J, from Fig. 5(b), and the electron density profile data, which gives the decay rate of 57 kW. If we take into account that the bulk electron temperature profile would not reach to a steady state for
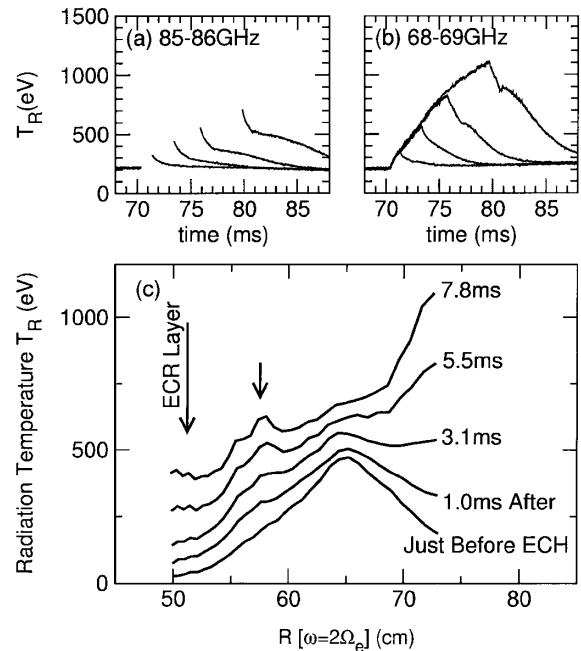

FIG. 4. (a), (b) Temporal evolution of ECE signals at $R[\omega \simeq 2\Omega_e] = 57.5$ and 72 cm for various ECH pulse lengths. (c) Radial radiation temperature profiles from ECE signals.
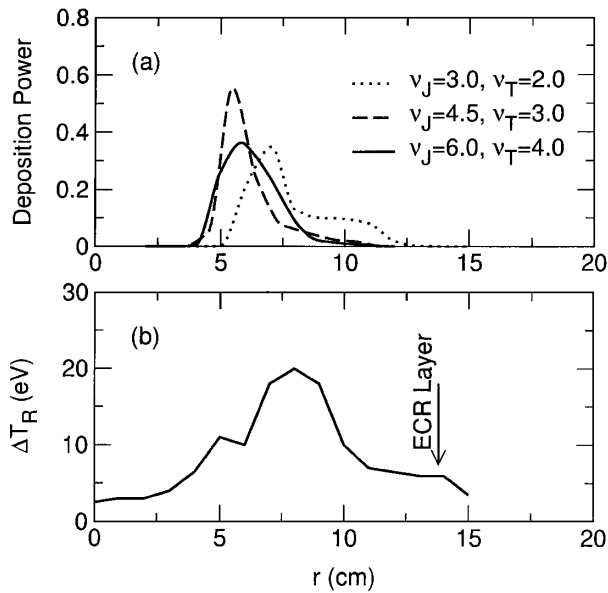
FIG. 5. Radial profiles of (a) B wave power deposition from multiray calculation and (b) decremental ECE radiation temperature. Calculation parameters are $n_0 = 2.16 \times 10^{13}$ cm^{-3}, $T_0 = 480$ eV, $I_p = 60$ kA, and $\nu_n = 2$.

the present short pulse and take the observed decay time τ_d as the energy confinement time, the corrected power, which should be balanced with the absorbed power, is estimated to be 85 kW for the present injection power of $P_{EC} \simeq 100$ kW. These results suggested that the injected X waves are efficiently mode converted to the B waves, which are absorbed by Doppler-shifted cyclotron resonance via $N_\parallel$ upshift. The peripheral electron temperature may be higher than the radiation temperature, since the optical depth is low at periphery. If we employ the Spitzer resistivity for the radiation temperature profile just before ECH in Fig. 4(c), the central safety factor is estimated to be $q_0 \simeq 0.7$, but no sawteeth appear in these high edge q_a ($\simeq 7$) discharges. Sawteeth appear for the discharges in the range of $q_a < 5.5$. Therefore, in the ray calculations we use the current profile indices in the range of $\nu_J = 3$–6, which gives $q_0 = 1$–1.75. The change of radiation temperature ΔT_R due to the change of local temperature ΔT_e is given by $\Delta T_R = \Delta T_e \{1 + (\tau - 1) \exp(-\tau)\}$, where τ is the optical depth and proportional to the local T_e. This formula gives $\Delta T_R / \Delta T_e = 0.7 \sim 1.15$ for the peak region in Fig. 5(b), where $\tau > 0.5$. Therefore, the estimated absorption power for the temperature change is approximately correct.

The change of $N_\parallel$ of B waves near the UHR layer is approximately analyzed as follows. The refractive index perpendicular to the toroidal direction, $\vec{N}$, increases quickly during the mode conversion process and the B wave rays leave the UHR layer perpendicularly as shown in Fig. 3(a). The vector $\vec{N}$ is also perpendicular to the layer but its direction is opposite to the ray direction. Therefore, the poloidal component N_p near the UHR layer is given by $N_p / N = \hat{s} \cdot \hat{\theta} = \sin\theta (2\beta \partial\beta / \partial R) / |\nabla S|$. Here, $\hat{s}$ is the unit vector perpendicular to the UHR layer and $\hat{\theta}$ the unit vector parallel to the poloidal field, θ is the poloidal angle measured from the midplane, $S = 1 - \alpha - \beta^2$, $\alpha = \omega_{pe}^2 / \omega^2$, and $\beta = \Omega_e / \omega$. At the UHR layer, $S = 0$. Thus, $N_\parallel = N_p B_p / B_t$ stems from the gradient of the toroidal field $B_t \propto R^{-1}$ along the poloidal direction and increases as $\sin\theta$ increases. An estimation of $N_\parallel$ of B waves near the UHR layer is obtained by substituting the dispersion relation of B waves in the warm plasma approximation, $N^2 = (\frac{2}{3})(c/v_t)^2 S(1 - 4\beta^2)/\alpha$, into the above relations. Especially, there would be no $N_\parallel$ upshift, if B wave rays were on the midplane. Thermal emission of B waves from the ECR layer was reported in this configuration [9].

In summary, we have shown that B waves are efficiently mode converted from X waves and absorbed midway between the UHR and ECR layers, consistently with the ray tracing prediction, i.e., the poloidal field and the poloidal inhomogeneity of toroidal field lead B waves having a large parallel refractive index $N_\parallel$ and B waves are damped away by Doppler-shifted cyclotron resonance.

[1] H. P. Laqua, V. Erckmann, H. J. Hartfus, H. Laqua, W7-AS Team, and ECRH Group, Phys. Rev. Lett. **78**, 3467 (1997).
[2] H. P. Laqua, H. J. Hartfus, and W7-AS Team, Phys. Rev. Lett. **81**, 2060 (1998).
[3] P. C. Efthimion, J. C. Hosea, R. Kaita, R. Majeski, and G. Taylor, Rev. Sci. Instrum. **70**, 1018 (1999).
[4] S. D. Schultz, A. K. Ram, and A. Bers, in the *Proceedings of the Conference on Fusion Energy, Yokohama, 1998* (International Atomic Energy Agency, Vienna, 1999), Vol. 2, p. 667.
[5] C. B. Forest, P. K. Chattopadhyay, R. W. Harvey, and A. P. Smirnov, Phys. Plasmas **7**, 1352 (2000).
[6] H. Sugai, Phys. Rev. Lett. **47**, 1899 (1981).
[7] T. Maekawa, S. Tanaka, Y. Terumichi, and Y. Hamada, J. Phys. Soc. Jpn. **48**, 247 (1980).
[8] A. G. Litvak, E. V. Suvorov, and M. D. Tokman, Phys. Lett. A **188**, 64 (1994).
[9] J. Hosea, V. Arunasalam, and R. Cano, Phys. Rev. Lett. **39**, 408 (1977).